TECHNICAL MEMORANDUM

716

Approximate Stokes Drift Profiles in Deep Water

Øyvind Breivik, Peter A.E.M. Janssen and Jean-Raymond Bidlot

Research Department

12 December 2013

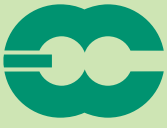

European Centre for Medium-Range Weather Forecasts
Europäisches Zentrum für mittelfristige Wettervorhersage
Centre européen pour les prévisions météorologiques à moyen terme

Series: ECMWF Technical Memoranda

A full list of ECMWF Publications can be found on our web site under:
http://www.ecmwf.int/publications/

Contact: library@ecmwf.int

European Centre for Medium-Range Weather Forecasts
Shinfield Park, Reading, RG2 9AX, England

Abstract

A new approximation to the Stokes drift velocity profile is proposed as an alternative to the monochromatic profile. Comparisons with parametric spectra and full two-dimensional wave spectra from the ERA-Interim reanalysis in the North Atlantic show significant improvement over the monochromatic profile even for complex sea states. The profile gives both a closer match and a more correct shear compared to the monochromatic profile. This has implications for ocean circulation since the Coriolis-Stokes force depends on the magnitude and direction of the Stokes drift profile and Langmuir turbulence depends sensitively on the shear of the profile. The proposed profile comes at no added numerical cost and relies on the same two parameters, viz the Stokes transport and the surface Stokes drift velocity.

1 Introduction

With the inclusion of Langmuir turbulence (Skyllingstad and Denbo 1995, McWilliams *et al.* 1997, Thorpe 2004, Ardhuin and Jenkins 2006, Grant and Belcher 2009 and Belcher *et al.* 2012) and Coriolis-Stokes forcing (Hasselmann 1970, Weber 1983, Jenkins 1987, McWilliams and Restrepo 1999, Janssen *et al.* 2004, Polton *et al.* 2005 and Janssen 2012) in Eulerian ocean models it becomes important to model the magnitude and the shear of the Stokes drift velocity correctly. Stokes drift profiles are also needed when estimating the drift of partially or entirely submerged objects (see McWilliams and Sullivan 2000, Breivik *et al.* 2012, Röhrs *et al.* 2012 and references in Breivik *et al.* 2013 for applications of Stokes drift velocity estimates for particle and object drift). However, computing the Stokes drift profile is expensive since it involves evaluating an integral with the two-dimensional wave spectrum at every desired vertical level. It is also often impractical or impossible since the full 2-D wave spectrum may not be available.

Here we propose an alternative approximate Stokes profile which will be compared to what is known as the monochromatic profile (Sec 2). The proposed profile was recently implemented in the ECMWF version of the NEMO ocean model (Madec, 2008) (the coupled forecast system and the coupling between the wave model and the ocean model components are described by Janssen *et al.* (2013)). This paper is organized as follows. In Sec 3 we investigate how these two approximate profiles compare for three well-known parametric spectra. Sec 4 examines the impact of a high-frequency spectral cut-off on the Stokes drift profile and the Stokes transport. This has implications for the computation of profiles from discretized spectra from numerical wave prediction models (Hasselmann *et al.*, 1988; Tolman, 1991; Komen *et al.*, 1994; Booij *et al.*, 1999; Ris *et al.*, 1999; Tolman *et al.*, 2002; Janssen, 2004). We investigate how well the proposed profile fits the full profiles computed from two-dimensional wave spectra from the ERA-Interim reanalysis (Dee *et al.*, 2011) in Sec 5. Here we also quantify how much waves beyond the high-frequency cut-off affect the shear and the magnitude of the Stokes drift profile. Furthermore we investigate the impact of approximating the Stokes transport direction by the more readily available mean wave direction as well as approximating the magnitude of the Stokes transport vector by the first order moment. Finally, in Sec 6 we present our recommendations for the computation of approximate Stokes profiles.

2 Approximate Stokes Drift Profiles

The Stokes drift profile in water of arbitrary depth was shown by Kenyon (1969) to relate to the wave spectrum as

$$\mathbf{u}_s(z) = g \int\int_{-\infty}^{\infty} F(\mathbf{k}) \frac{\mathbf{k}}{\omega} \left[\frac{2k \cosh 2k(z+d)}{\sinh 2kd} \right] \mathrm{d}\mathbf{k}, \tag{1}$$

where $k = |\mathbf{k}|$ is the magnitude of the wavenumber vector, d is the bottom depth (positive), g the gravitational acceleration, $\omega = 2\pi f$ the circular frequency and z is the vertical co-ordinate (positive up). In the following we will only consider the deep-water limit of the dispersion relation,

$$\omega^2 = gk. \tag{2}$$

Then Eq (1) simplifies to

$$\mathbf{u}_s(z) = \frac{2}{g} \int\int_{-\infty}^{\infty} \omega^3 \hat{\mathbf{k}} e^{2kz} F(\mathbf{k}) \, \mathrm{d}\mathbf{k}, \tag{3}$$

where $\hat{\mathbf{k}} = \mathbf{k}/k$ is the unit vector in the direction of the wave component.

We now recast the east and north components of the Stokes drift profile in frequency-direction (f,θ) co-ordinates as

$$\mathbf{u}_\mathrm{s}(z) = \frac{16\pi^3}{g}\int_0^{2\pi}\int_0^{\infty} f^3\hat{\mathbf{k}}\mathrm{e}^{2kz}F(f,\theta)\,\mathrm{d}f\mathrm{d}\theta, \tag{4}$$

where θ is measured clockwise from north (going to) and $f = \omega/2\pi$.

The Stokes transport $\mathbf{T}_\mathrm{s} = \int_{-\infty}^{0}\mathbf{u}_\mathrm{s}(z)\,dz$ becomes in the deep-water limit

$$\mathbf{T}_\mathrm{s} = 2\pi\int_0^{2\pi}\int_0^{\infty} f\hat{\mathbf{k}}F(f,\theta)\,\mathrm{d}f\mathrm{d}\theta. \tag{5}$$

The integrand here is the first-order moment of the wave spectrum, m_1, weighted by the unit vector $\hat{\mathbf{k}}$ of the wave component, with the n-th order moment of the 2-D spectrum defined as

$$m_n = \int_0^{2\pi}\int_0^{\infty} f^n F(f,\theta)\,\mathrm{d}f\mathrm{d}\theta. \tag{6}$$

Estimating the full profile from Eq (4) can be a costly operation even when a modeled or observed wave spectrum is available. When a wave spectrum is not available the Stokes profile must be approximated from the transport (Eq 5) and the surface Stokes drift velocity. It is therefore customary to approximate Eq (4) by the exponential profile of a monochromatic wave (see eg Skyllingstad and Denbo 1995; McWilliams and Sullivan 2000; Carniel *et al.* 2005; Rascle *et al.* 2006; Saetra *et al.* 2007; Tamura *et al.* 2012)

$$u_\mathrm{m} = u_0\mathrm{e}^{2k_\mathrm{m}z}. \tag{7}$$

To ensure that the surface Stokes drift and the total transport of the monochromatic wave in Eq (7) agree with the values for the full spectrum, Eqs (4)-(5), the wavenumber must be determined by

$$k_\mathrm{m} = \frac{u_0}{2T_\mathrm{s}}. \tag{8}$$

We have explored an alternative to the exponential profile of the form

$$u_\mathrm{e} = u_0\frac{\mathrm{e}^{2k_\mathrm{e}z}}{1-8k_\mathrm{e}z}. \tag{9}$$

The transport under such a profile involves the exponential integral E_1 and can be solved analytically (Abramowitz and Stegun 1972, **5.1.28**) to yield

$$T_\mathrm{s} = \frac{u_0\mathrm{e}^{1/4}E_1(1/4)}{8k_\mathrm{e}}. \tag{10}$$

It will in the following be referred to as the exponential integral profile. This imposes the following constraint on the wavenumber,

$$k_\mathrm{e} = \frac{u_0\mathrm{e}^{1/4}E_1(1/4)}{8T_\mathrm{s}}. \tag{11}$$

Here $E_1(1/4)\approx 1.34$, thus

$$k_\mathrm{e} \approx \frac{u_0}{5.97T_\mathrm{s}} \approx k_\mathrm{m}/3. \tag{12}$$

We will now assess the quantitative and qualitative differences between the two approximate profiles, referred to by subscripts *m* for monochromatic and *e* for exponential integral.

3 Profiles under Parametric Spectra

Under a one-dimensional spectrum in the deep-water limit Eq (4) becomes

$$u_s(z) = \frac{2}{g}\int_0^\infty \omega^3 F(\omega) e^{2\omega^2 z/g}\, d\omega. \tag{13}$$

We now introduce the Phillips spectrum (Phillips, 1958, 1985; Janssen, 2004), applicable to the equilibrium range of the spectrum of wind-generated waves above the spectral peak,

$$F_P = \begin{cases} \alpha_P g^2 \omega^{-5}, & \omega > \omega_p \\ 0, & \omega \le \omega_p \end{cases}, \tag{14}$$

Here we set Phillips' parameter $\alpha_P = 0.0083$ (there is some disagreement about its values with others workers, including Holthuijsen 2007 and Webb and Fox-Kemper 2011 preferring the value 0.0081). The peak circular frequency is denoted ω_p. The Stokes profile under the Phillips spectrum is

$$u_P(z) = 2\int_{\omega_p}^\infty \alpha_P g \omega^{-2} e^{2\omega^2 z/g}\, d\omega. \tag{15}$$

The transport under this Stokes profile can be found analytically, yielding

$$T_P = \frac{\alpha_P g^2}{3\omega_p^3}. \tag{16}$$

Eq (15) is compared with the two approximate profiles (Eqs 7 and 9) in Panel a of Fig 1. The exponential integral approximation has a root-mean-square (rms) error of about a sixth that of the monochromatic approximation.

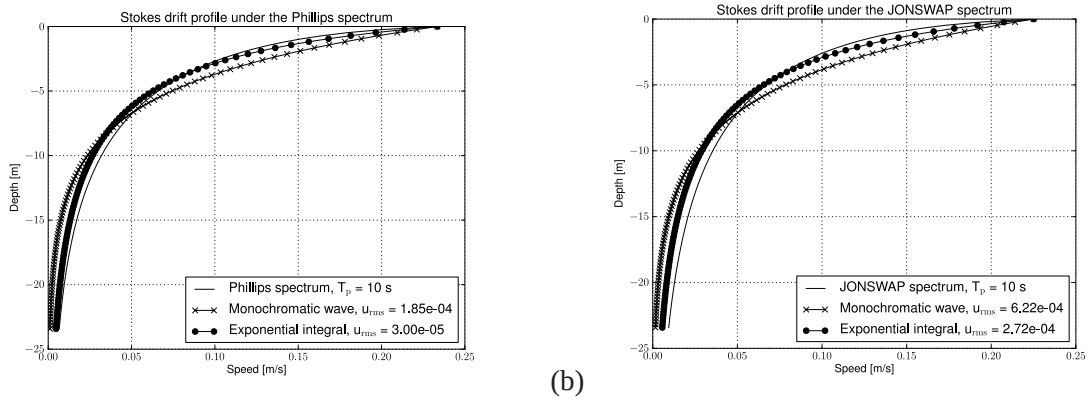

(a) (b)

Figure 1: Panel a: The Stokes drift profile under the Phillips spectrum ($T_p = 10$ s). The monochromatic approximation (x) tends to overestimate the drift in the upper part of the water column while underestimating the drift in the deeper part. The exponential integral approximation (o) exhibits closer correspondence throughout the water column, with an rms error about six times smaller than that found for the monochromatic approximation. Panel b: The Stokes drift profile under the JONSWAP spectrum ($T_p = 10$ s). The results are similar to those for the Phillips spectrum with an rms error of the exponential integral (o) about 60% times smaller than that of the monochromatic approximation (x).

The Pierson-Moskowitz (P-M) spectrum (Pierson and Moskowitz, 1964) is commonly used to model fully developed (equilibrium) sea states,

$$F_{PM} = \alpha_P g^2 \omega^{-5} \exp\left[-\frac{5}{4}\left(\frac{\omega_p}{\omega}\right)^4\right]. \tag{17}$$

We find the same general improvement as was found for the Phillips spectrum above with an rms error about a fifth that of the monochromatic approximation (not shown). Note that here the integral covers also the lower frequencies as the spectrum remains bounded for all frequencies. Panel b shows the profile under the JONSWAP spectrum. This spectrum is based on the P-M spectrum with a peak enhancement to account for the spectral shape found in fetch-limited seas (Hasselmann *et al.*, 1973; Janssen, 2004; Webb and Fox-Kemper, 2011)

$$F_{\text{JONSWAP}} = F_{\text{PM}}\gamma^{\Gamma}, \tag{18}$$

where

$$\Gamma = \exp\left[-\frac{1}{2}\left(\frac{f/f_{\text{p}}-1}{\sigma}\right)^2\right]. \tag{19}$$

Here typical values are $\gamma = 3.3$, $\sigma = 0.07$ for $f \leq f_{\text{p}}$ and $\sigma = 0.09$ when $f > f_{\text{p}}$. The exponential integral profile gives a reduction in rms of about 60% compared with the monochromatic profile.

3.1 The Shear of the Stokes Profile

The production of Langmuir turbulence arises from a vortex force term, $\mathbf{u_s} \times \nabla \times \mathbf{u}$, in the momentum equation (Leibovich, 1983). The vortex force gives rise to a term involving the *shear* of the Stokes drift velocity profile in the turbulence kinetic energy (Kantha and Clayson 2004, Polton and Belcher 2007, Grant and Belcher 2009, Belcher *et al.* 2012 and Janssen 2012). This is illustrated below in a simplified version of the TKE equation where lateral gradients and advective terms are ignored,

$$\frac{\partial e}{\partial t} = \nu_{\text{m}} S^2 + \nu_{\text{m}}\mathbf{S}\cdot\frac{\partial \mathbf{u}_{\text{s}}}{\partial z} - \nu_{\text{h}} N^2 - \frac{1}{\rho_{\text{w}}}\frac{\partial}{\partial z}(\overline{p'w'}) - \frac{\partial}{\partial z}(\overline{ew'}) - \varepsilon. \tag{20}$$

Here $e = q^2/2$ is TKE per unit mass, with q the turbulent velocity. We recognize the familiar terms of the TKE equation [see Stull 1988, Eq (5.1a)], namely shear production, $S^2 = (\partial\overline{\mathbf{u}}/\partial z)^2$, and buoyancy production, $N^2 = -(g/\rho)d\rho/dz$ ($\nu_{\text{m,h}}$ are turbulent diffusion coefficients for momentum and heat, respectively) as well as the divergences of the pressure correlation term $\overline{p'w'}$ and the turbulent transport $\overline{ew'}$ and finally the dissipation ε. The term involving the shear vector $\mathbf{S} = \partial\overline{\mathbf{u}}/\partial z$ multiplied with the shear of the Stokes profile represents production of Langmuir turbulence.

It is of interest to investigate the shear under parametric spectra, and for the Phillips spectrum (15) an analytical solution can be found (Gradshteyn and Ryzhik 2007, **3.321.2**),

$$\frac{\partial u_{\text{P}}}{\partial z} = 2\alpha_{\text{P}} g\int_{\omega_{\text{p}}}^{\infty} \mathrm{e}^{-2\omega^2|z|/g}\,\mathrm{d}\omega = \sqrt{\frac{\pi g}{8|z|}}\,\mathrm{erfc}\left(\sqrt{\frac{2|z|}{g}}\omega_{\text{p}}\right). \tag{21}$$

On the surface the shear goes to infinity. This is in contrast to the shear under a monochromatic wave (7), which remains bounded near the surface,

$$\frac{\partial u_{\text{m}}(z=0)}{\partial z} = 2k_{\text{m}}u_0. \tag{22}$$

The shear of the exponential integral profile (9) also remains bounded, but reaches a 50% higher value than the monochromatic profile at the surface,

$$\frac{\partial u_{\text{e}}(z=0)}{\partial z} = 10k_{\text{e}}u_0 \approx \frac{10}{3}k_{\text{m}}u_0. \tag{23}$$

Technically the singularity in Eq (21) can be avoided by moving the computation of the Stokes shear away from the surface through the use of a staggered grid, but it remains an open question whether the current understanding of Langmuir turbulence production is adequate.

4 High-frequency contribution to the profile

The same procedure as outlined above can be used to compute the profiles and transports from discretized wave spectra with a high-frequency cut-off. However, as the Stokes drift is weighted toward the high-frequency (HF) part of the spectrum, the tail beyond the cut-off frequency (f_c) is significant both for the profile and the transport. We follow Komen *et al.* (1994) pp 233–234 and assume a tail of the form

$$F_{\mathrm{HF}} = F(f_c,\theta)\left(\frac{f_c}{f}\right)^5, \tag{24}$$

which is consistent with the Phillips spectrum (14). The two-dimensional spectrum below the cut-off frequency is here assumed to come from observations or from a numerical wave prediction model. This is the procedure used for adding the diagnostic high-frequency contribution to the spectrum in the WAM model, see Hasselmann *et al.* 1988; Komen *et al.* 1994; Janssen 2004; ECMWF 2012 as well as the WaveWatch-III model, Tolman 1991; Tolman *et al.* 2002).

The high-frequency tail adds the following contribution,

$$\mathbf{u}_{\mathrm{HF}}(z) = \frac{16\pi^3}{g} f_c^5 \int_0^{2\pi} F(f_c,\theta)\hat{\mathbf{k}}\,\mathrm{d}\theta \int_{f_c}^{\infty} \frac{\exp(8\pi^2 z f^2/g)}{f^2}\,\mathrm{d}f. \tag{25}$$

The latter integral can be solved analytically (see eg Gradshteyn and Ryzhik 2007, **3.461.5**), yielding

$$\mathbf{u}_{\mathrm{HF}}(z) = \frac{16\pi^3}{g} f_c^5 \int_0^{2\pi} F(f_c,\theta)\hat{\mathbf{k}}\,\mathrm{d}\theta \left[\frac{\exp(-\mu f_c^2)}{f_c} - \sqrt{\mu\pi}\,(1-\mathrm{erf}(f_c\sqrt{\mu}))\right], \tag{26}$$

where $\mu = -8\pi^2 z/g$. The high-frequency addition to the surface Stokes drift in deep water can be found by setting $\mu = 0$, which simplifies to

$$\mathbf{u}_{\mathrm{HF}}(0) = \frac{16\pi^3}{g} f_c^4 \int_0^{2\pi} F(f_c,\theta)\hat{\mathbf{k}}\,\mathrm{d}\theta. \tag{27}$$

The ECMWF WAM model (ECMWF, 2012) computes and outputs the surface Stokes drift velocity vector corrected for the high-frequency contribution.

The tail contribution to the transport becomes

$$\mathbf{T}_{\mathrm{HF}} = \frac{2\pi}{3} f_c^2 \int_0^{2\pi} F(f_c,\theta)\hat{\mathbf{k}}\,\mathrm{d}\theta. \tag{28}$$

5 Modeled Profiles in the North Atlantic

The ERA-Interim is a continuously updated atmospheric and wave field reanalysis produced by the European Centre for Medium-Range Weather Forecasts (ECMWF) starting in 1979. The model and data assimilation scheme of the reanalysis are based on Cycle 31r2 of the Integrated Forecast System (IFS). The wave model WAM is coupled to the atmospheric part of the IFS (see Janssen 2004 for details of the coupling and Dee *et al.* 2011 for an overview of the ERA-Interim reanalysis). The resolution of the wave model model component is 1.0° on the Equator but the resolution is kept approximately constant globally through the use of a quasi-regular latitude-longitude grid where grid points are progressively removed toward the poles (Janssen, 2004). A similar scheme applies for the atmospheric component, but here

the resolution is approximately 0.75° at the Equator. The wave model is run with shallow water physics where appropriate. The spectral range from 3.45×10^{-2} to 0.55 Hz is spanned with 30 logarithmically spaced frequency bands. The angular resolution is 15°.

For this study we computed the Stokes profiles down to 30 m depth from the two-dimensional ERA-Interim spectra in a region in the north Atlantic ocean (59 – 60°N, 20 – 19°W, see Fig 2) for the whole

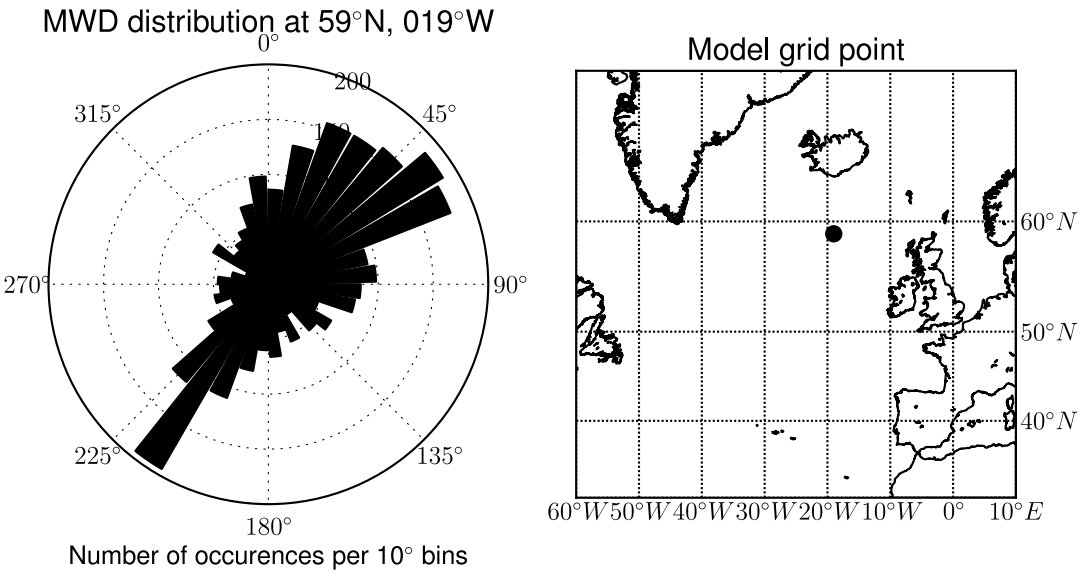

Figure 2: Left panel: The directional distribution of the mean wave direction (going to) in model location 59° N, 019° W. A large spread in wave direction is found. The location has a high prevalence of wind sea but is also exposed to swell. Right panel: Model location.

of 2010. This region is stormy while also exposed to swell, providing a range of complex wave spectra. To assess the difference between the monochromatic approximation and the exponential integral approximation the rms deviation from the full Stokes profile to 30 m depth was calculated for every spectrum. The results are shown in Fig 3. The rms deviation of the exponential integral profile from the full Stokes profile is on average 35% that of the monochromatic profile for our chosen location and model period (2010). The improvement is consistent for a range of different sea states, as illustrated in Fig 4. In Panel a the match is so close that the exponential integral profile overlaps the full profile. Poor performance is expected in cases where a one-dimensional fit is made to wave spectra with two diametrically opposite wave systems. Such a case is shown in Panel b, where a swell system travels in the opposite direction of the wind sea. Indeed, this spectrum represents the worst fit found throughout the model period, but even

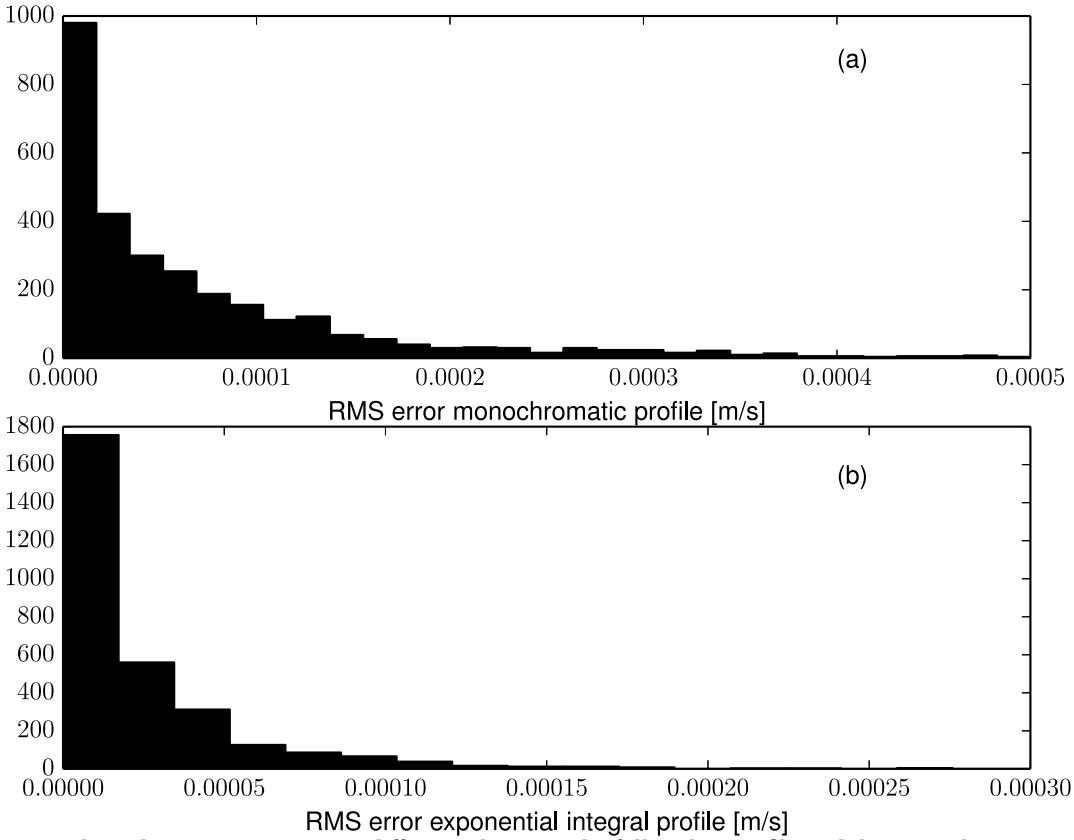

Figure 3: Panel a: The root-mean-square difference between the full Stokes profile and the monochromatic profile to 30 m depth (vertical resolution 0.1 m). Panel b: The rms difference of the exponential integral profile is on average about one third that of the monochromatic profile shown in Panel a.

here there is slight improvement over the monochromatic approximation. The rms and bias of the *shear* of the Stokes drift profiles estimated over the water column to 30 m depth were found to be on average 66% and 55% that of the monochromatic profile.

5.1 High-frequeny Contribution to Stokes Drift

The contribution from the spectral tail to the surface Stokes drift velocity found in Eq (26) is on average about a third, and sometimes exceeding 75% (Fig 5, Panel a). It is well known that adding the contribution from the high-frequency tail is important, and indeed it is standard practice to include it in the computation of the surface Stokes drift velocity (see eg the ECMWF model documentation, ECMWF 2012, p 52). In contrast, its contribution to the *transport* is generally marginal (average 3%, Panel b, Fig 5), although in certain cases it may exceed 10%. The high-frequency contribution decays rapidly with depth, as can be seen in Panel a of Fig 6. Below 0.5 m the difference between the low-frequency (LF) profile and the full profile is marginal. Neither of the approximate profiles is a particularly good match, but of the two the exponential integral profile has a slightly better gradient than the monochromatic profile. This mismatch in the upper half meter is in contrast to the good overall match found for the whole water column (see Fig 4). This means that the contribution from Langmuir turbulence near the surface (Eq (20)) will be underestimated. Panel b shows the approximate profiles with the high-frequency contribution added. Now the gradient is much closer to that of the theoretical full Stokes profile. In

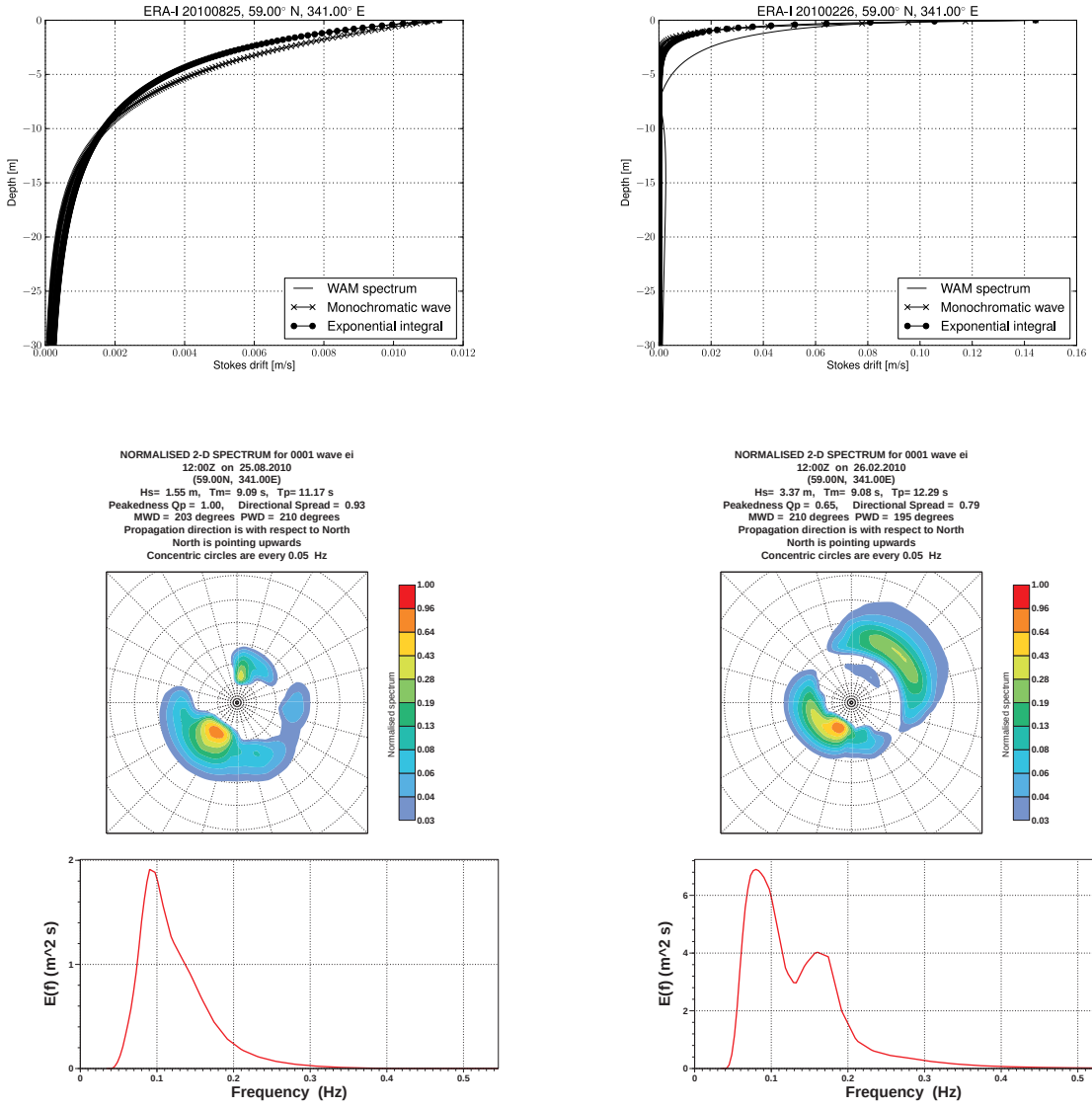

(a) (b)

Figure 4: Panel a: The Stokes drift profile under a full two-dimensional wave spectrum from the ERA-Interim reanalysis. The location is in the north Atlantic. An extremely good fit is found in this case. The 2-D spectrum shows a strong bimodality which is masked in the 1-D spectrum. Panel b: Much poorer fit is found in this case where a strong swell system is superimposed on locally generated wind sea. There is still some improvement over the monochromatic approximation. Here the swell part is dominant and of a lower frequency, making the 1-D spectrum bimodal.

principle it is straightforward to add this contribution to the approximate profile by way of Eq (26), but it requires knowledge of the two-dimensional wave spectrum at the cut-off frequency f_c.

The Stokes transport (28) is also affected by the high frequency contribution, although much less so (about 10%, see Fig 5, Panel b), which is to be expected since the transport is a function of the first moment.

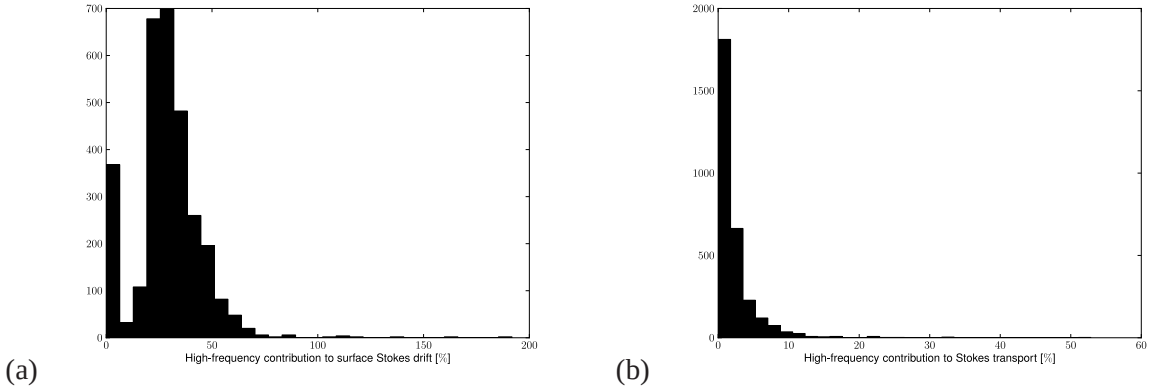

(a) (b)

Figure 5: Panel a: Ratio of high-frequency contribution to the surface Stokes drift. On average the contribution is about 39%. Panel b: Ratio of high-frequency contribution to the Stokes transport. On average the contribution is about 3%, and only occasionally will it exceed 10%.

5.2 Discrepancy Between the Stokes Transport and m_1

It is clear that

$$|\mathbf{T}_s| \leq 2\pi m_1, \tag{29}$$

but it is not clear how large this deviation is on average for typical wave spectra in the open ocean. Assessing the overestimation is of practical value since the first spectral moment is often archived or indirectly measured. Since the mean frequency is defined as $\overline{f} = m_1/m_0$ (World Meteorological Organization, 1998; Holthuijsen, 2007) and the significant wave height $H_{m_0} = 4\sqrt{m_0}$, we can derive the first moment from the integrated parameters of a wave model or from wave observations and find an estimate for the Stokes transport,

$$\mathbf{T}_s \approx \frac{2\pi}{16}\overline{f}H_{m_0}^2\hat{\mathbf{k}}_s. \tag{30}$$

Here $\hat{\mathbf{k}}_s = (\sin\theta_s, \cos\theta_s)$ is the unit vector in the direction θ_s of the Stokes transport.

Note that this Stokes transport direction is not normally archived by wave prediction models, but it can be approximated by the mean wave direction $\overline{\theta}$ as will be shown later. Estimating the Stokes transport from the first moment is attractive since it involves only integrated parameters readily available from wave models. Fig 7 shows good correspondence between the the Stokes transport and the estimate based on m_1 in Eq (30) with a correlation coefficient of 0.96, but m_1 will overestimate the transport on average by 16%. Both transport estimates include the contribution from the diagnostic high-frequency spectral tail.

5.3 Deviation between the Stokes transport direction and the mean wave direction

The mean wave direction (MWD) measured clockwise from North in the direction the waves are propagating to is defined as

$$\overline{\theta} = \arctan\left(\frac{\int_0^{2\pi}\int_0^{\infty}\sin\theta F(f,\theta)\,\mathrm{d}f\mathrm{d}\theta}{\int_0^{2\pi}\int_0^{\infty}\cos\theta F(f,\theta)\,\mathrm{d}f\mathrm{d}\theta}\right). \tag{31}$$

It is of interest to assess how well it approximates the direction of the Stokes transport since it is a standard output parameter of many wave models (ECMWF, 2012) whereas the Stokes transport is generally

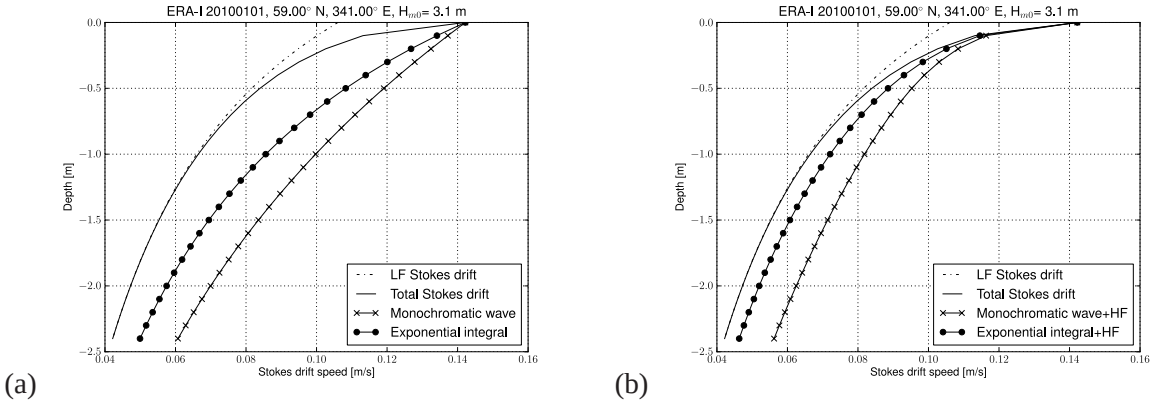

Figure 6: Panel a: The high-frequency contribution to the Stokes drift velocity. The Short waves beyond the cut-off frequency contribute only to the drift in the upper half meter (compare the dash-dotted low-frequency Stokes drift to the total drift drawn with a full line). The two approximate profiles are pegged to the surface Stokes drift and coincide exactly at the surface. The shear is not well represented by either of the approximate profiles in the upper half meter, but the exponential integral profile is the better match of the two. Panel b: The same approximate profiles with the high-frequency profile added. A much better match for the upper meters of the ocean is achieved, both in terms of shear and absolute error.

not. Panel a of Fig 8 shows the deviation of the Stokes transport from the MWD in the model location in the north Atlantic during 2010. The average deviation is about 2° and 75% of the time the difference is less than 10°. In contrast, Panel b shows a much larger deviation between the direction of the Stokes transport and the surface Stokes drift velocity. This is due to the sensitivity to high-frequency wave components arising from the third power of the frequency f under the integral in Eq (4). It will therefore in general be better to estimate the transport direction from the mean wave direction rather than from the surface Stokes direction.

6 Recommendations for Approximate Stokes Profiles

The alternative profile proposed here has been shown to be a better approximation than the monochromatic approximation for both theoretical spectra and numerically estimated spectra in the open ocean. Utilizing this alternative profile comes at no added cost since the computation relies on the same two parameters required for the monochromatic profile, namely the Stokes transport, $\mathbf{T}_S$, and the surface Stokes drift velocity, $\mathbf{u}_0$. We also found that in the open ocean the mean wave direction serves as a good proxy for the Stokes transport direction. It is a significantly better substitute than the surface Stokes drift direction. Furthermore, the one-dimensional first order moment, m_1, is found to correlate well with the magnitude of the two-dimensional transport, $|\mathbf{T}_S|$. A factor of 0.86 (16% reduction) seems appropriate in open ocean conditions.

Discretized spectra add a diagnostic high-frequency tail, see Eq (24). We find that adding the contribution from the tail gives an important contribution to the Stokes drift velocity in the upper half meter in the open ocean. Its impact rapidly decays, and below 0.5 m the difference is marginal (Panel a, Fig 6). This has implications for the computation of the gradient of the Stokes drift in the uppermost part of the ocean. Neither of the approximate profiles match the gradient in the upper half meter well, and this is important to keep in mind for future studies of upper-ocean turbulence. We note again that although it is

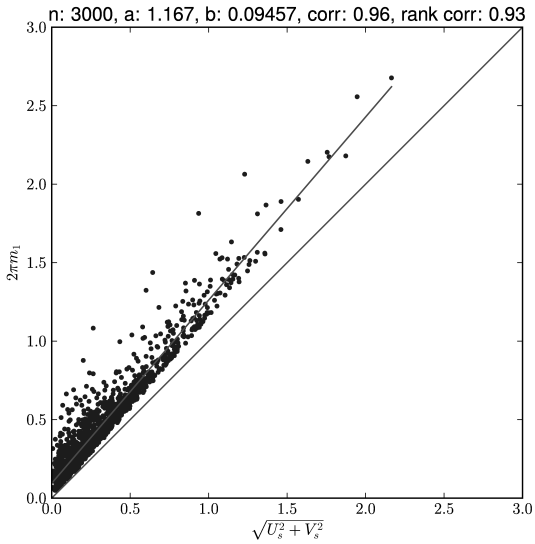

Figure 7: The discrepancy between the two-dimensional Stokes transport $|\mathbf{T}_s|$ and the unidirectional estimate $2\pi m_1$ from the ERA-Interim reanalysis. Good agreement is generally found, but the unidirectional estimate will on average be 16% too high.

numerically inexpensive to add the high-frequency contribution to the profile, its reliance on the full 2-D spectrum makes this approach impractical for applications where the spectrum is unavailable.

We conclude that the proposed Stokes profile is a closer match than the commonly used monochromatic profile both in terms of speed and shear. Although both profiles poorly match the real shear in the upper half meter, even here the new profile offers a slight improvement over the monochromatic profile. As Langmuir turbulence depends sensitively on the Stokes drift shear the question of whether approximate profiles can be found that more closely mimic the gradient in the uppermost half meter merits further work.

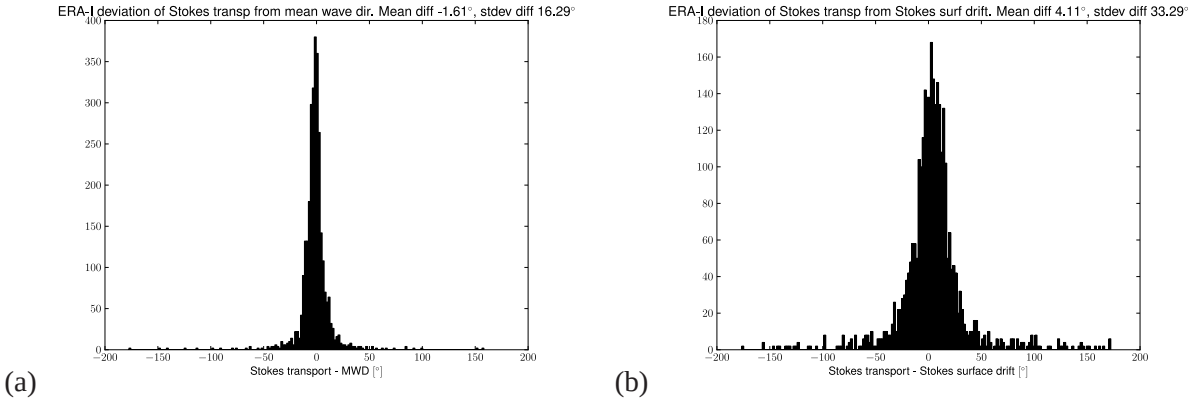

(a) (b)

Figure 8: Panel a: The directional deviation between the Stokes transport and the mean wave direction (MWD). The average deviation is about 2° *and 75% of the time the difference is less than* 10°*. Panel b: The directional deviation between the Stokes transport and the surface Stokes drift velocity is larger due to the* f^3 *weighting of the wave spectrum which gives larger weight to high-frequency wave components.*

Acknowledgment

This work has been carried out with support from the European Union FP7 project MyWave (grant no 284455).

References

Abramowitz M, Stegun IA (eds). 1972. *Handbook of Mathematical Functions, with Formulas, Graphs, and Mathematical Tables*. Dover: New York.

Ardhuin F, Jenkins A. 2006. On the Interaction of Surface Waves and Upper Ocean Turbulence. *J Phys Oceanogr* **36**: 551–557, doi:10.1175/2009JPO2862.1.

Belcher SE, Grant ALM, Hanley KE, Fox-Kemper B, Van Roekel L, Sullivan PP, Large WG, Brown A, Hines A, Calvert D, Rutgersson A, Pettersson H, Bidlot JR, Janssen PAEM, Polton JA. 2012. A global perspective on Langmuir turbulence in the ocean surface boundary layer. *Geophys Res Lett* **39**(18): L18 605, 9 pp, doi:10.1029/2012GL052 932.

Booij N, Ris RC, Holthuijsen LH. 1999. A third-generation wave model for coastal regions 1. Model description and validation. *J Geophys Res* **104**(C4): 7649–7666, doi:10.1029/98JC02 622.

Breivik Ø, Allen A, Maisondieu C, Olagnon M. 2013. Advances in Search and Rescue at Sea. *Ocean Dynam* **63**(1): 83–88, doi:10.1007/s10 236–012–0581–1, doi:10/jtx, arXiv:1211.0805.

Breivik Ø, Allen A, Maisondieu C, Roth JC, Forest B. 2012. The Leeway of Shipping Containers at Different Immersion Levels. *Ocean Dynam* **62**(5): 741–752, doi:10.1007/s10 236–012–0522–z, doi:10/fzw885, arXiv:1201.0603.

Carniel S, Sclavo M, Kantha LH, Clayson CA. 2005. Langmuir cells and mixing in the upper ocean. *Il Nuovo Cimento C Geophysics Space Physics C* **28C**: 33–54, doi:10.1393/ncc/i2005–10 022–8.

Dee D, Uppala S, Simmons A, Berrisford P, Poli P, Kobayashi S, Andrae U, Balmaseda M, Balsamo G, Bauer P, P B, Beljaars A, van de Berg L, Bidlot J, Bormann N, *et al.* 2011. The ERA-Interim reanalysis: Configuration and performance of the data assimilation system. *Q J R Meteorol Soc* **137**(656): 553–597, doi:10.1002/qj.828.

ECMWF. 2012. IFS Documentation CY38r1, Part VII: ECMWF Wave Model. ECMWF Model Documentation, European Centre for Medium-Range Weather Forecasts.

Gradshteyn I, Ryzhik I. 2007. *Table of Integrals, Series, and Products, 7th edition*. Edited by A. Jeffrey and D. Zwillinger, Academic Press, London.

Grant AL, Belcher SE. 2009. Characteristics of Langmuir turbulence in the ocean mixed layer. *J Phys Oceanogr* **39**(8): 1871–1887, doi:10.1175/2009JPO4119.1.

Hasselmann K. 1970. Wave-driven inertial oscillations. *Geophysical and Astrophysical Fluid Dynamics* **1**(3-4): 463–502, doi:10.1080/03091927009365 783.

Hasselmann K, Barnett TP, Bouws E, Carlson H, Cartwright DE, Enke K, Ewing JA, Gienapp H, Hasselmann DE, Kruseman P, Meerburg A, Müller P, Olbers DJ, Richter K, Sell W, Walden H. 1973. Measurements of wind-wave growth and swell decay during the Joint North Sea Wave Project (JONSWAP). *Dtsch Hydrogr Z* **A8**(12): 1–95.

Hasselmann S, Hasselmann K, Bauer E, Janssen PAEM, Komen GJ, Bertotti L, Lionello P, Guillaume A, Cardone VC, Greenwood JA, Reistad M, Zambresky L, Ewing JA. 1988. The WAM model—a third generation ocean wave prediction model. *J Phys Oceanogr* **18**: 1775–1810.

Holthuijsen L. 2007. *Waves in Oceanic and Coastal Waters*. Cambridge University Press.

Janssen P. 2004. *The interaction of ocean waves and wind*. Cambridge University Press, Cambridge, UK.

Janssen P. 2012. Ocean Wave Effects on the Daily Cycle in SST. *J Geophys Res* **117**: C00J32, 24 pp, doi:10/mth.

Janssen P, Breivik Ø, Mogensen K, Vitart F, Balmaseda M, Bidlot J, Keeley S, Leutbecher M, Magnusson L, Molteni F. 2013. Air-Sea Interaction and Surface Waves. ECMWF Technical Memorandum 712, European Centre for Medium-Range Weather Forecasts.

Janssen P, Saetra O, Wettre C, Hersbach H, Bidlot J. 2004. Impact of the sea state on the atmosphere and ocean. In: *Annales hydrographiques*, vol. 3-772. Service hydrographique et océanographique de la marine, pp. 3.1–3.23.

Jenkins AD. 1987. Wind and wave induced currents in a rotating sea with depth-varying eddy viscosity. *J Phys Oceanogr* **17**: 938–951, doi:10/fdwvq2.

Kantha LH, Clayson CA. 2004. On the effect of surface gravity waves on mixing in the oceanic mixed layer. *Ocean Modelling* **6**(2): 101–124, doi:10.1016/S1463–5003(02)00 062–8.

Kenyon KE. 1969. Stokes Drift for Random Gravity Waves. *J Geophys Res* **74**(28): 6991–6994, doi:10.1029/JC074i028p06 991.

Komen GJ, Cavaleri L, Donelan M, Hasselmann K, Hasselmann S, Janssen PAEM. 1994. *Dynamics and modelling of ocean waves*. Cambridge University Press: Cambridge.

Leibovich S. 1983. The form and dynamics of Langmuir circulations. *Ann Rev Fluid Mech* **15**(1): 391–427, doi:10.1146/annurev.fl.15.010 183.002 135.

Madec G. 2008. Nemo ocean engine. Note du Pole de modélisation 27, Institut Pierre Simon Laplace.

McWilliams J, Sullivan P, Moeng CH. 1997. Langmuir turbulence in the ocean. *J Fluid Mech* **334**(1): 1–30, doi:10.1017/S0022112096004 375.

McWilliams JC, Restrepo JM. 1999. The Wave-driven Ocean Circulation. *J Phys Oceanogr* **29**(10): 2523–2540, doi:10/dwj9tj.

McWilliams JC, Sullivan PP. 2000. Vertical mixing by Langmuir circulations. *Spill Science and Technology Bulletin* **6**(3): 225–237, doi:10.1016/S1353–2561(01)00 041–X.

Phillips OM. 1958. The equilibrium range in the spectrum of wind-generated waves. *J Fluid Mech* **4**: 426–434, doi:10.1017/S0022112058000 550.

Phillips OM. 1985. Spectral and statistical properties of the equilibrium range in wind-generated gravity waves. *J Fluid Mech* **156**: 505–531, doi:10.1017/S0022112085002 221.

Pierson Jr WJ, Moskowitz L. 1964. A proposed spectral form for fully developed wind seas based on the similarity theory of S A Kitaigorodskii. *J Geophys Res* **69**: 5181–5190.

Polton JA, Belcher SE. 2007. Langmuir turbulence and deeply penetrating jets in an unstratified mixed layer. *J Geophys Res* **112**(C9): 11, doi:10.1029/2007JC004 205.

Polton JA, Lewis DM, Belcher SE. 2005. The role of wave-induced Coriolis-Stokes forcing on the wind-driven mixed layer. *J Phys Oceanogr* **35**(4): 444–457, doi:10.1175/JPO2701.1.

Rascle N, Ardhuin F, Terray E. 2006. Drift and mixing under the ocean surface: A coherent one-dimensional description with application to unstratified conditions. *J Geophys Res* **111**(C3): C03 016, 16pp, doi:10.1029/2005JC003 004.

Ris RC, Holthuijsen LH, Booij N. 1999. A third-generation wave model for coastal regions 2. Verification. *J Geophys Res* **104**(C4): 7667–7681, doi:10.1029/1998JC900 123.

Röhrs J, Christensen K, Hole L, Broström G, Drivdal M, Sundby S. 2012. Observation-based evaluation of surface wave effects on currents and trajectory forecasts. *Ocean Dynam* **62**(10–12): 1519–1533, doi:10.1007/s10 236–012–0576–y.

Saetra Ø, Albretsen J, Janssen P. 2007. Sea-State-Dependent Momentum Fluxes for Ocean Modeling. *J Phys Oceanogr* **37**(11): 2714–2725, doi:10.1175/2007JPO3582.1.

Skyllingstad ED, Denbo DW. 1995. An ocean large-eddy simulation of Langmuir circulations and convection in the surface mixed layer. *J Geophys Res* **100**(C5): 8501–8522, doi:10.1029/94JC03 202.

Stull RB. 1988. *An introduction to boundary layer meteorology*. Kluwer: New York.

Tamura H, Miyazawa Y, Oey LY. 2012. The Stokes drift and wave induced-mass flux in the North Pacific. *J Geophys Res* **117**(C8): 14, doi:10.1029/2012JC008 113.

Thorpe S. 2004. Langmuir Circulation. *Annu Rev Fluid Mech* **36**: 55–79, doi:10.1146/annurev.fluid.36.052 203.071 431.

Tolman HL. 1991. A Third-Generation Model for Wind Waves on Slowly Varying, Unsteady, and Inhomogeneous Depths and Currents. *J Phys Oceanogr* **21**(6): 782–797.

Tolman HL, Balasubramaniyan B, Burroughs LD, Chalikov DV, Chao YY, Chen HS, Gerald VM. 2002. Development and Implementation of Wind-Generated Ocean Surface Wave Models at NCEP. *Wea Forecasting* **17**(2): 311–333, doi:10/d74ttq.

Webb A, Fox-Kemper B. 2011. Wave spectral moments and Stokes drift estimation. *Ocean Modelling* **40**: 273–288, doi:10.1016/j.ocemod.2011.08.007.

Weber J. 1983. Steady Wind- and Wave-Induced Currents in the Open Ocean. *J Phys Oceanogr* **13**: 524–530, doi:10/djz6md.

World Meteorological Organization. 1998. Guide to wave analysis and forecasting.